Flomo L. Gbawoquiya[1], Kumari Rachna[1], Shankara S. Narayanan[2], Pramod K. Singh[2], Shiv Shankar[3], Ikhwan Syafiq Mohd Noor[4], Muhd Zu Azhan Yahya[5]*

[1]Department of Environmental Sciences, Sharda School of Basic Sciences & Research, Sharda University, Greater Noida, India, [2]Department of Physics, Sharda School of Basic Sciences & Research, Sharda University, Greater Noida, India.[3]Department of Environmental Science,School of Vocational Studies and Applied Sciences, Gautam Buddha University, Greater Noida, India.[4]Physics Division, Centre of Foundation Studies for Agricultural Sciences, Universiti Putra Malaysia, UPM Serdang, 43400 Selangor Darul Ehsan, Malaysia, [5]Faculty of Defence Science and Technology, Universiti Petrahanan Nasional Malaysia (UPNM), 57000 Kuala Lumpur, Malaysia.

Scientific paper
ISSN 0351-9465, E-ISSN 2466-2585
https://doi.org/10.62638/ZasMat1201

Zastita Materijala 65 (3)
452 - 465 (2024)

Facile Synthesis and adsorptive removal of Rhodamine B dye from aqueous medium using green synthesized nanocomposite

ABSTRACT

Reduced graphene oxide (rGO) and zinc oxide nanoparticles (ZnO NPs) were synthesized using modified Hummer's method and green approach from Carica papaya leaf extract (CPLE), respectively. ZnO NPs were then loaded onto rGO using a straightforward ultrasonic method to synthesize Zinc oxide-reduced graphene oxide nanocomposite (ZnO-rGO NC). Fourier Transform Infrared Spectroscopy (FTIR), Field Emission Scanning Electron Microscopy (FESEM), and X-ray diffraction (XRD) techniques were used to characterize the synthesized nanoparticles and composite respectively. The nanocomposite was used to remove Rhodamine B dye (RhB) from aqueous solution. The effects of temperature, pH, adsorbent dosage, initial dye concentration, and contact time were investigated. Testing was done on the Freundlich and Langmuir isotherm models as well and the thermodynamics parameters were computed. The effects of ZnO NPs, rGO, and ZnO-rGO NC independently on dye removal in a comparative analysis were carried out and resulteds were presented. In an aqueous medium, the nanocomposite demonstrated high removal efficiency as an adsorbent for removing RhB dye at 99% compared to ZnO NPs at 60%. ZnO-rGO NC proved to be an effective adsorbent compare to ZnO NPs.

Keywords: *Adsorption, ZnO nanoparticles, nanocomposites, pollutants, rhodamine b, reduced graphene oxide, carica papaya*

1. INTRODUCTION

The textile dyeing and printing industry is one of the major global polluters and consumers of water resources at this moment in time [1]. Globally, more than a million tonnes of dyes are generated each year; processing one tonne of textiles would need 100–200 tonnes of water, and 80–90% of the wastewater emitted is made up of organic dye wastewater [2].

The introduction of wastewater tainted with highly colored dyes into natural watersheds will reduce the transparency of water bodies and hinder the growth of native species. Moreover, conventional fixation techniques usually include mordents comprising heavy metals to improve the color rapidity of dyed fabrics because some colorants have poor affinities for fibers [3].

Long-term exposure to heavy metals and organic pollutants in wastewater can also lead to the malignant mutation of other species [4]. Consequently, the intricacy of the real effluent should not be underestimated while treating water.

To increase the efficacy of color removal, ZnO has also been used. Nanocomposites are used as a result of the agglomeration of nanoparticles, but ZnO-rGO NC stands out due to its wide surface area and high adsorption effectiveness. Of all the semiconductors employed in photocatalysis, ZnO has shown itself to be a practical choice [5]. Its direct bandgap allows it to be triggered by energy in the near-UV range and gives it excellent photocatalytic activity [6]. Furthermore, ZnO is an environmentally benign, biocompatible, and non-toxic material.

Due to its large band gap (3.37 eV) and high exciton binding energy (60 meV), zinc oxide (ZnO) has attracted a lot of interest for application in nanoscale electrical and optoelectronic devices [7]. It is also commonly known that ZnO, a polar crystal

Corresponding author: Kumari Rachna
E-mail: km.rachna@sharda.ac.in;
Paper received: 13. 01. 2024.
Paper accepted: 19. 02. 2024.
Paper is available on the website: www.idk.org.rs/journal

with significant anisotropy, develops along the c-axis due to its hexagonal phase. ZnO is a great replacement for TiO_2 in terms of band energy [8]. ZnO NPs are used in a broad variety of industrial applications, such as laser active medium, fluorescent tube luminescence material, sensors, and antibacterial agents [9].

Harmful chemical organic dyes that leak into rivers and groundwater are the result of most modern industries, especially those in the food, cosmetics, paint, cellulose, plastic, textile, and livestock farming sectors [10]. Not only do these materials not biodegrade, but they also pollute the environment, endanger human health, and harm the natural balance of bodies of water [11]. Because of this, during the past few years, researchers have focused on developing safe, alternate green, physical, and chemical methods for removing organic dyes from wastewater. Adsorption is a simple, low-energy, chemical-free method that has recently gained traction in the environmental treatment industry [12]. Due to poor exploitation of natural water resources, faster industrialization, insufficiently planned urbanization, and rising population growth, there are significant water safety challenges today [13]. Essentially, biomass—such as waste from forestry and agriculture—could be pyrolyzed to produce adsorbents that effectively extract toxic substances from wastewater [14]. Many modification approaches (e.g., chemical and physical activation techniques) have been reported to efficiently enhance the pore structure and adsorption sites, resulting in the creation of novel adsorbent materials with optical, electrical, and magnetic properties [15]. Several inexpensive and easily accessible experimental studies have been conducted recently [16]. The textile industry makes extensive use of RhB dye. It can be removed with an absorbent. RhB is widely used in a variety of sectors; however, it is also highly toxic and carcinogenic. It is hard for it to decompose in water and can cause a host of ailments, such as cancer, genetic issues, organ damage, and anemia. Although RhB is banned in many countries, it is nonetheless used illegally as a textile dye and food additive in several developing countries. It is utilized in this investigation because of its notable status as an environmental pollutant.

The Carica papaya L. plant, which is a member of the Caricaceae family, is widely used as a remedy all over the world, particularly in tropical and subtropical regions. In traditional medicine, several elements of the C. papaya plant, including the leaves, bark, roots, latex, fruit, flowers, and seeds, are used to cure a range of illnesses [17]. It has been used in the synthesis of nanoparticles recently, in addition to the existing uses. The green synthesis process is straightforward, energy-efficient, environmentally benign, and non-toxic, among its numerous advantages over chemical methods. As a result, there is increasing interest in synthesizing ZnO nanoparticles for essential applications using a narrow particle size distribution through a green approach. For example, Koupaei et al. reported synthesizing ZnO NPs utilizing extract from coffee powder and investigated the impact of ZnO NPs on proteinase K's secondary structure, enzyme activity, and thermal stability [18]. The outer peel extract of *C. paradise* was used by Brajesh Kumar et al. to prepare the spherical ZnO NPs, which were then employed as photocatalysts to degrade the dye methylene blue (MB) and increase their antioxidant activity. Notably, they demonstrated 56% degradation efficiency against MB dye over a 6-hour exposure period [19]. Additionally, a few attempts have also been undertaken to synthesize crystalline ZnO NPs utilizing plant extracts from *Physalis alkekengi L.* and *Sedum alfredii Hance* [20, 21]. Given their accessibility, ability to produce nanoparticles in large quantities, and environmentally benign waste products compared to some microbe extracts among other biological extracts, plants or their extracts appear to be the ideal agents [22, 23]. Plant extracts contain phyto components that have a variety of benign and adaptable actions, including acting as reducing and stabilizing agents simultaneously [24, 25].

In this work, zinc oxide was synthesized using Carica papaya leaves. The phytochemicals in the plant extract served as reducing agents during the synthesis process, transforming the metal precursors into metal nanoparticles. Because they are free of toxins and antioxidants, phytochemicals can function as both stabilizing and reducing agents. Flavonoids and alkaloids for instance, are phytochemicals found in Carica papaya leaf extract that aid in the reduction of zinc ions. According to Love et al., to stabilize metal ions following reduction by the *C. papaya* leaf extract, they will be encapsulated as an organic coating in three phases throughout the synthesis process: The first phase is called the activation phase, during which metal ions reduce and their nucleation occurs. 2. Growth Phase: during this time, the nanoparticle becomes stable, and 3. Termination Phase: the nanoparticles' shape is formed at this stage [26]. Using a straightforward ultrasonic-assisted method, the synthesized nanoparticles were combined with reduced graphene oxide (rGO) to form a composite. Therefore, the goals of this work are to purify water using ZnO-rGO NC by green method.

2. MATERIALS AND METHODS

2.1. Materials

Zinc acetate dihydrate $[CH_3OO]_2$ $Zn.2H_2O$ (Fisher Scientific) with purity 99%, Sodium Nitrate $[NaNO_3]$(Fisher Scientific) with purity 99.99%, Sulfuric acid $[H_2SO_4]$ (Somadi) with purity 98.0%, Hydrogen peroxide $[H_2O_2]$ (Somadi) with purity 30.0%, Acetone$[(CH_3)_2CO]$ (Somadi) with purity 99%, Hydrochloric acid [HCl] (Somadi) with purity 99%, Potassium permanganate [KMnO4] (Fisher Scientific) with 98.5%, Sodium hydroxide [NaOH] (Somadi) with 97% purity, Thiourea $[NH_2CSNH_2]$ and Rhodamine b dye $[C_{28}H_{31}ClN_2O_3]$ were used.

2.2. Methods

2.2.1. Preparation of Plant

CPLE were washed, cut into small pieces, dried, and later boiled with 100mL distilled water for 30 min. 10 grams of the *CPLE* was used for boiling. The extract obtained was filtered using Whatman No. 1 and kept in a refrigerator which was subsequently used.

2.2.2. Synthesis of ZnO Nanoparticles

Double deionized water (DDW) was used to prepare 50 mL of 0.1 M of zinc acetate dihydrate. 10 mL of *CPLE* was slowly added drop-wise to the solution at 80 ^oC, stirred magnetically for 4 hours, and adjusted to pH 12. The resulting mixture was centrifuged at 10,000 rpm for 10 min. the pellet was washed and centrifuged at 5000 rpm for 10 min. The washed pellets obtained after centrifugation were dried at 50 ^oC for 6 hrs and Calcined in a muffle furnace at 450 ^oC to synthesize zinc oxide NPs [27, 28].

2.2.3. Synthesis of Reduced Graphene Oxide

Graphite powder was oxidized using a modified Hummer's method [29]. In an ice bath, a combination of pre-oxidized graphite (3 g), $NaNO_3$ (1.5 g), and H_2SO_4 (115 mL) was stirred for 20 minutes. $KMnO_4$ (9 g) was slowly added to the suspension and stirred vigorously with a constant temperature at (>20 °C). The temperature of the solution was further increased to 35 °C and stirred continuously for close to 12 hours. In addition, 300 mL DDW was added after the temperature of the precursor solution was increased to 98 °C. The residual manganese dioxide and permanganate were then removed from the suspension using (30% weight) colorless H_2O_2 after it had been diluted with 1L of DDW. The pH of the mixture was neutralized by filtering and washing repeatedly with (5% weight) HCl aqueous solution and DDW, respectively. The mixture was then vacuum-dried for 24 hours at 40 °C to produce the finished form of GO. The obtained GO was combined with the reducing agent (Thiourea) at 100 °C for roughly 24 hours with constant stirring, yielding rGO [30].

2.2.4. Formation of rGO/ZnO Nanocomposite

The ZnO-rGO NC was synthesized using a simple ultrasonic-assisted solution method. 1 g of rGO was sonicated for 30 minutes with 150 mL DDW. Similarly, 0.25 g of ZnO was mixed with 50 mL DDW and sonicated for 30 minutes separately. Both solutions were then combined and sonicated for 45 minutes before being stirred constantly for 1 hour and dried in a hot air oven. The ZnO-rGO NC powder was finally obtained [30].

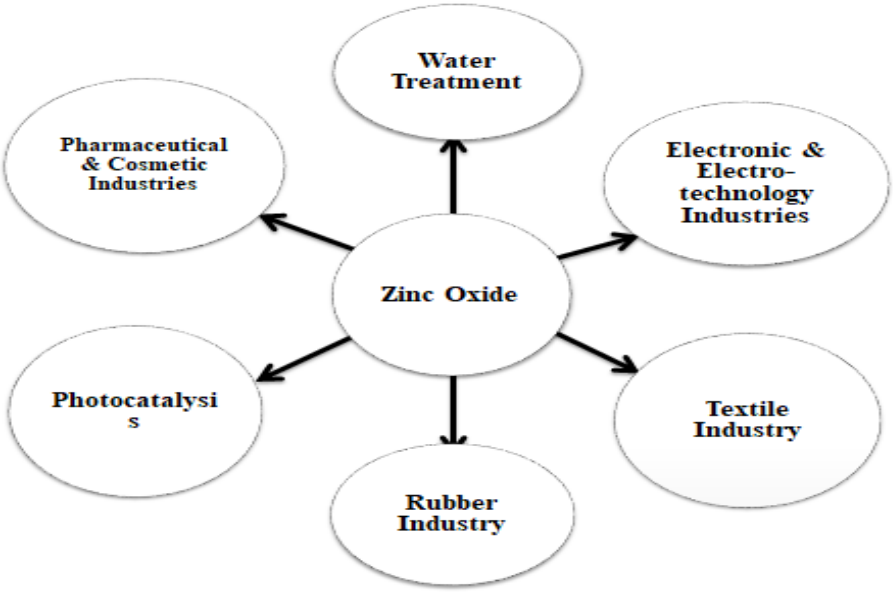

Figure 1. Utilization of ZnO in other disciplines

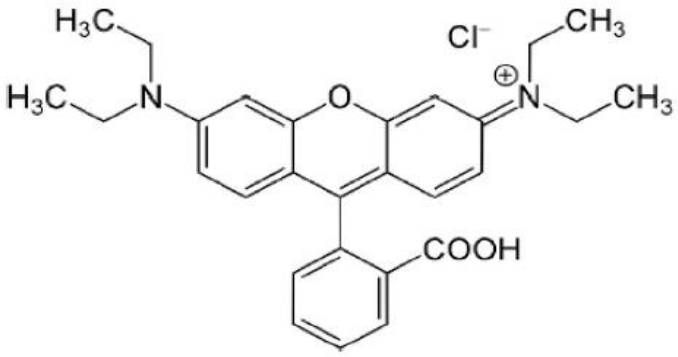

Figure 2. Main properties and chemical makeup of RhB

2.2.5. Preparation RhB Dye Solution

A 10 ppm stock solution of RhB dye was prepared using a 10 mg/L dye. 1L of distilled water was used to dissolve the RhB dye. Different concentrations were prepared from the stock solution as follows: 2, 4, 6, and 8 ppm.

2.2.6. X-ray Diffraction Studies

ZnO and ZnO-rGO NC XRD investigations were conducted using an X-ray diffractometer with CuKα radiation between 2θ=5–600. This adaptable apparatus is intended for a broad range of uses in X-ray diffraction examination on powders, thin films, epitaxial layers, machined materials, ceramics, etc. The user can switch the system from a high resolution or stress texture point focus application to a standard Bragg-Brentano line focus configuration or a reflectometry system by utilising the pre-FIX optical modules, sample platform, and tube rotation capability.

2.2.7. FESEM studies

ZnO, rGO, and ZnO-rGO nanocomposite FESEM images were captured. With its ultra-high resolution characterization and analysis, the FESEM-Nova Nano FE-SEM 450 (FEI) delivers accurate, real nanoscale scale data. The greatest information selection and picture optimization are provided by advanced optics and detection, including beam deceleration in lens ETD (SE), TLD (custom), lens-attached DBS, and LVD.

2.2.8. FTIR Spectrum Studies

ZnO NPs and rGO FTIR spectra were recorded. With its completely integrated, universal sampling system, the compact, user-friendly, and powerful FT-IR Spectrum 2 (Perkin Elmer) instrument can measure liquid (in KBr cells) and solid (in KBr pellets) samples in the 4100–400 cm-1 range. Pharmaceutical inventors and manufacturers, among others, can use it. Applications for it include spectral and field-based analysis, as well as infrared sampling.

2.9. Removal of RhB dye from Aqueous Medium

Using a UV-vis spectrophotometer, the UV-vis spectra of a 10 ppm RhB dye solution were recorded, allowing for the determination of λmax (553 nm). A calibration curve was produced after the absorbance at λ_{max} for solutions with various concentrations was established. At room temperature, 10 ppm, 20 mL of RhB dye solution, and (0.5g) of synthesized ZnO-rGO NC adsorbent were added and continuously stirred. Solutions were removed at various intervals of time (5, 10, 15, 20, 25, 30, 35, and 40 min), and the absorbance at λ_{max} was noted. The concentrations were determined using the calibration curve. Different concentrations of RhB dye solution were mixed with 0.5 g of adsorbent, and the amount extracted was measured at various times.

By adjusting with 0.1M HCl and 0.1M NaOH, dye removal was also investigated at various pH values. The percentage of dye removed was computed by the adsorbent using Eq. (1) [31].

$$Re\ (\%) = C_o - C_e / C_o \times 100 \quad (1)$$

At equilibrium, the amount of dye adsorbed, qe (mg/g), was calculated by Eq. (2).

$$q_e = (C_o - C_e)V/m \quad (2)$$

Where C_o and C_e represent initial and equilibrium dye concentrations, C_t represents the adsorbate initial concentrations, and V and m are the volume and mass of the solution and adsorbent respectively. q_t (mg/g), the amount adsorbed at time t is given by Eq. (3).

$$q_t = (C_o - C_t)V/m \quad (3)$$

Various doses of the ZnO-rGO nanocomposite (0.1 to 0.4 g) were employed to determine the percentage of dye removed at different concentrations. As shown in Fig. 3, it was found that the greatest removal happened at 0.4g. Based on these findings, a ZnO-rGO NC weighing 0.4g was employed to examine temperatures between 308—348K.

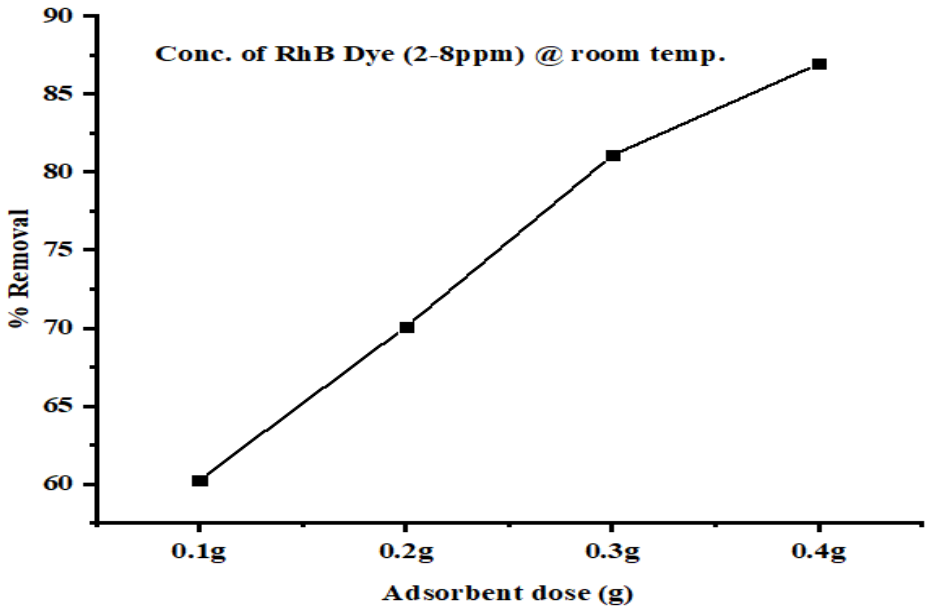

Figure 3. Percentage of RhB dye removed after 40 minutes from an aqueous medium with varying doses of ZnO-rGO NC at (10ppm)

3. RESULTS AND DISCUSSION

3.1. X-ray Diffraction

Fig. 4a shows the XRD pattern of ZnO NPs and ZnO-rGO NC. Appropriate planes: (100), (002), (101), (110), (103) and (112) were given to the characteristic diffraction peaks at 2Θ = 31.74°, 34.44°, 36.28°, 47.68°, 56.54°, 62.98° and 67.92°, accordingly, derived from the green synthesized composite of Carica papaya leaf. Equation (4) was utilized to calculate the crystallized size of ZnEO NPs by applying the Debye-Scherrer equation [32].

$$D = \frac{K\lambda}{\beta \cos\theta} \qquad (4)$$

where K is a constant (0.94), λ is the wavelength of *the X-ray* used, β is full width at half maxima (FWHM) and θ is Bragg angle. The average crystallite size was found to be 15.7 nm. The intensity of one peak at 2θ=37.74° is increased whereas the intensity of other peaks is much lower than that of ZnO-rGO NC. The formation of the nanocomposite was shown by a reduction in peak intensities in Figure 4b. ZnO-related diffraction peaks and rGO-related wide peaks are both visible in the ZnO-rGO NC XRD pattern. The rGO-ZnO NC XRD pattern offers evidence of the evolution of the hybridized structure.

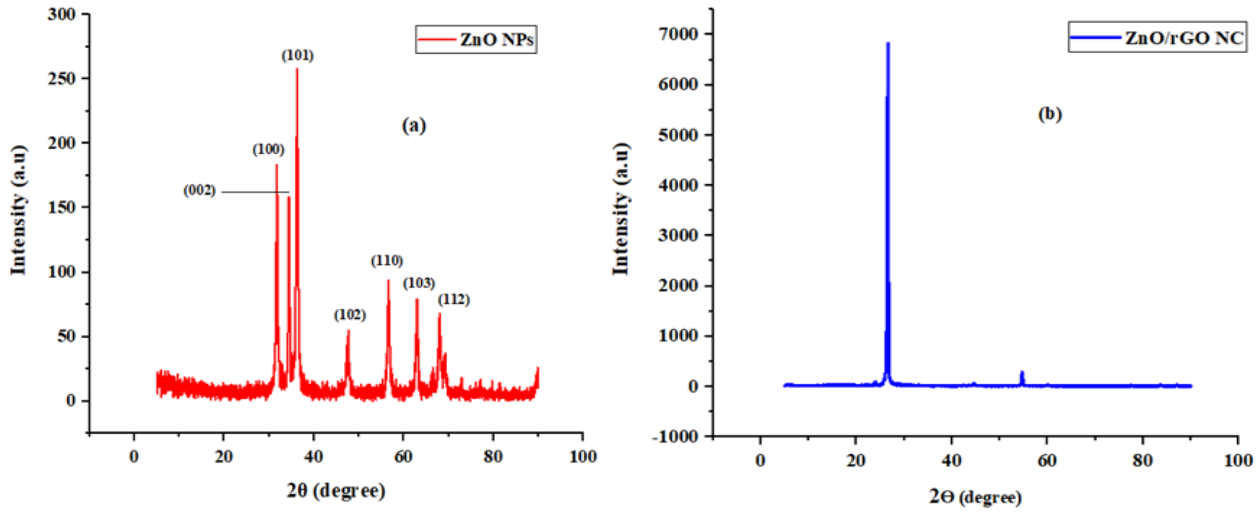

Figure 4. XRD spectra of (a) ZnO NPs (b) ZnO-rGO NC

3.2. FESEM studies

ZnO, rGO, and ZnO-rGO NC are shown in the images obtained from FESEM in (Fig 5). Sheet-like formations of rGO nanostructures were seen in (Fig. 5b). In (Fig. 5a), the ZnO indicates the formation of uniformly organized round structures whereas the ZnO-rGO NC displayed a group of scattered pellets across the plates that was noticed pointing to the composite assembled in the presence of zinc pellets and rGO plates(Fig.5c).

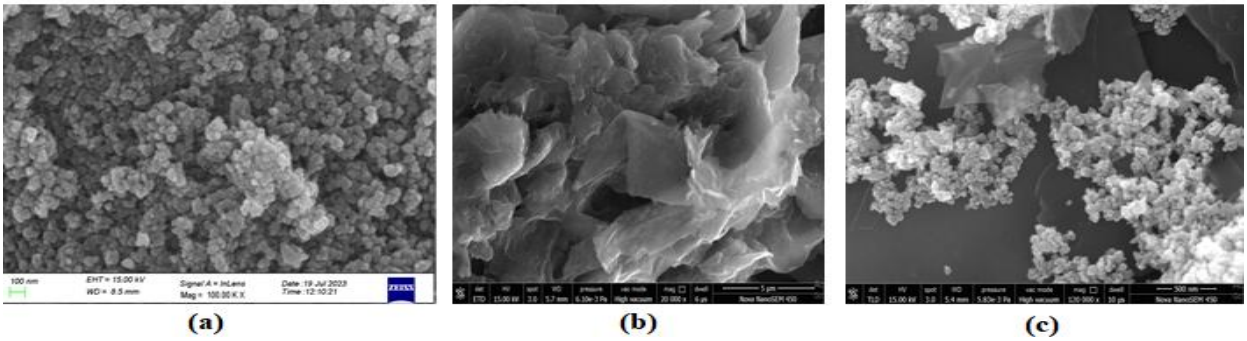

Figure 5. FESEM images of (a) ZnO (b) rGO and (c) ZnO-rGO NC

3.3. FTIR Spectrum

The FTIR spectra revealed a peak that was restricted to the area (500–4000 cm–1) of the spectrum (Fig. 6). The adsorption of water molecules is correlated with the vibration of OH at 3440 cm-1. Internal C-H stretching bonds are connected to the peak at 2949 cm-1 [33]. The peak at 1450 cm-1 is indicative of the adsorption's C-C bond. The stretching bond of 1270 cm-1 is connected to C-OH groups.

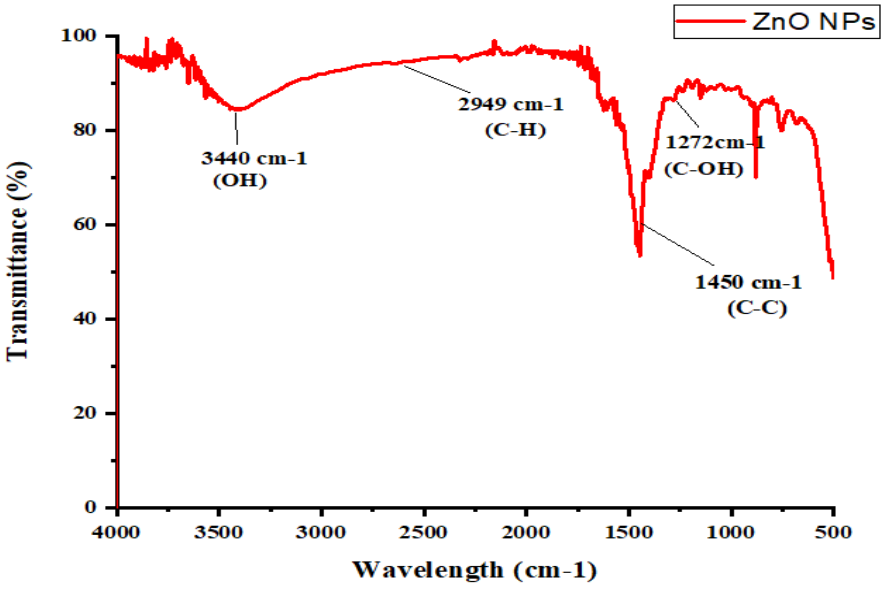

Figure 6. FTIR Spectrum of ZnO NPs

Table 1. Functional Group present in Green synthesized ZnO NPs analyzed by FTIR

S. no.	Absorption peak (cm−1) in ZnO NPs	Bond/Functional groups
1	3440	OH vibration
2	2949	C-H stretching bonds
3	1450	C-C bond
4	1272	C-OH

3.4. Tau Plot of ZnO NPs

Since the bandgap of a semiconductor has a significant impact on both its electrical and optical properties, the bandgap of ZnO NPs was determined using the Tau Plot. It is essential to comprehend ZnO NPs' bandgap to comprehend their behavior under various conditions. In (Fig. 7), the bandgap was observed at 3.085 eV; the nanoparticles offer helpful information for their applications in various fields. The measured band-gap correlates to green synthesized ZnO NPs previously disclosed in an investigation of a similar nature [34].

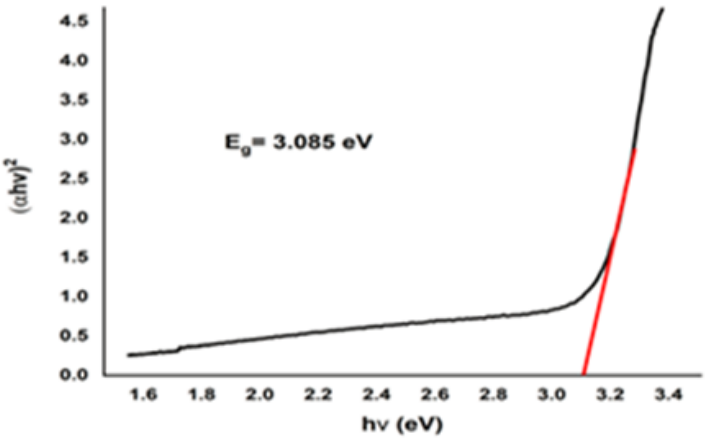

Figure 7. Tau Plot and Energy bandgap of ZnO NP

3.5. Adsorption of Rhodamine B Dye

3.5.1. The use of ZnO-rGO adsorbent for RhB Dye Removal concerning time

The duration of time required to remove RhB dye while using ZnO-rGO NC as the adsorbent was observed. Different times were observed for the dye's adsorption onto ZnO, rGO, and ZnO-rGO (Fig. 8). This was intended to study the removal capacity of ZnO, rGO, and ZnO-rGO NC comparatively. Within twenty-five minutes (25 min), maximum adsorption happened. The RhB dye was found to be adsorbed most maximally at 80% by ZnO-rGO NC, and least maximally at 60% by ZnO. The surface area was decreased because ZnO, a nanoparticle, may have likely agglomerated according to the result, hence, the low removal. 51% of the dye was removed by rGO, suggesting that rGO aggregation might have led to the creation of larger clusters, which would have limited the accessibility of active sites on the surface.

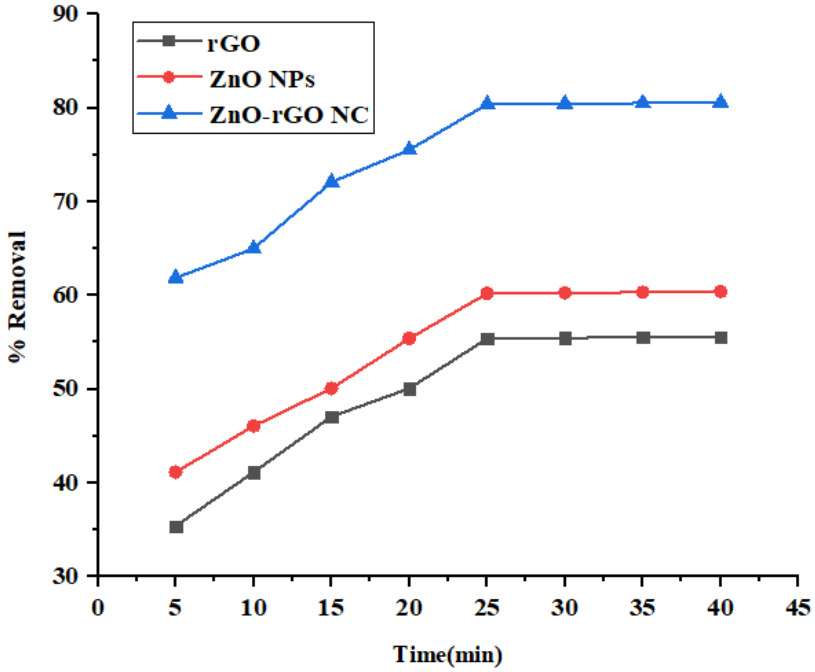

Figure 8. RhB dye Percent Removal from Aqueous Medium

An important factor in adsorption processes is how long the adsorbent/adsorbate interacts. The ZnO-rGO NC adsorbent's effectiveness is demonstrated by its rapid adsorbate absorption and quick equilibrium realization. After reaching equilibrium, further adsorption became quite challenging [35]. The adsorption of RhB dye with time in the presence of ZnO-rGO NC is shown in (Fig.9).

Figure 9. RhB Dye Adsorption utilizing ZnO-rGO NC for 5–40 min.

3.5.2. Dosage of the Absorbent and RhB Removal

The impact of ZnO-rGO NC dosage on the elimination of RhB dye at a constant dye concentration (10 ppm) is displayed in Fig. 10. With an increase in the adsorbent's quantity from (0.1 to 0.5 g/20 mL), the percentage of dye removed increased. According to Zhang et al. [36] assertion, with an increase in the overall adsorbent surface area and concurrent adsorption sites, dye removal increases as adsorbent dosage increases.

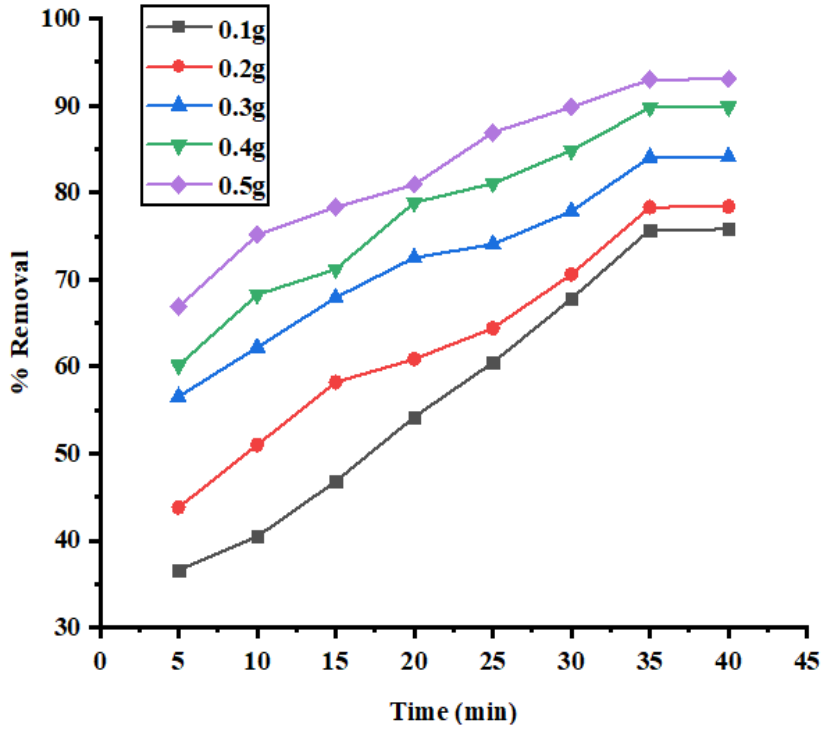

Figure 10. Impact of varying doses of ZnO-rGO NC for RhB Dye Removal

3.5.3. Impact of RhB dye Concentration on its Removal from Water at a constant ZnO-rGO Dosage

The removal of RhB dye from aqueous medium at several concentrations was investigated, and the results are shown in Fig. 11**.** The impact of a fixed dose of ZnO-rGO NC adsorbent (0.5 g ZnO-rGO/20 mL). The findings indicate that at a concentration of 2 ppm, the greatest elimination at 99% occurred after 40 minutes. It seems as though nearly all of the dye may be eliminated when there is little of the dye present in the aqueous medium and a large quantity of the ZnO-rGO NC adsorbent is present. What this means is that ZnO-rGO NC works well as an efficient adsorbent when there are remnants of RhB dye in an aqueous medium.

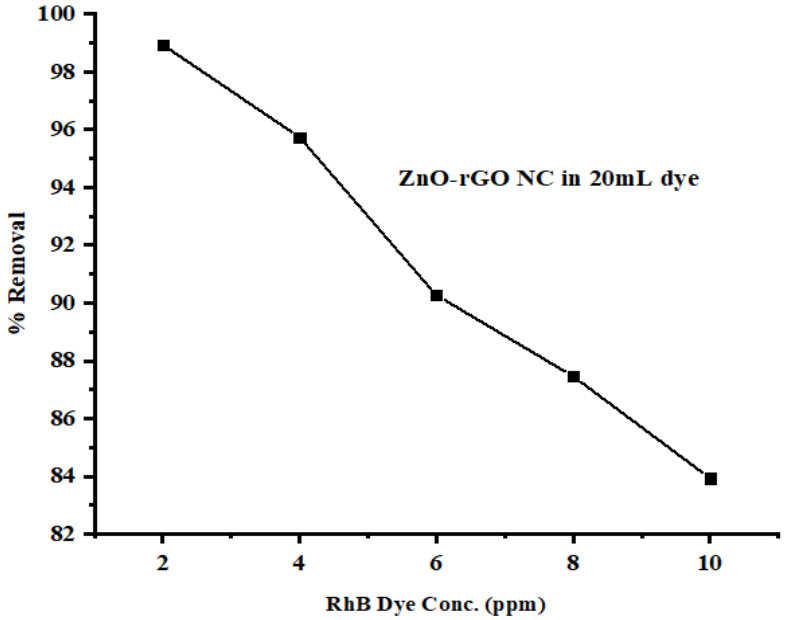

Figure 11. Impact of ZnO-rGO NC fixed Dose on RhB Dye Removal from the aqueous medium at varying conc. after 40 minutes

3.5.4. Effect of pH

In (Fig. 12), a pH range of 2 to 10 was investigated for ZnO-rGO's NC removal of RhB dye. Since pH impacts the adsorbent's surface charge characteristics and the way adsorbate ions behave in the solution, it is the most crucial parameter for assessing the efficacy of adsorption. The result shown indicates that the dye's greatest adsorption was attained at 80%. The proportion of dye elimination then sharply decreased from 80 to less than 10% at the moment when the pH increased from 2 to 10. What this implies is that the maximum rate might probably be obtained at a lower pH because RhB dye comes in a variety of forms, most notably zwitterionic and cationic. Another explanation for this phenomenon is an adsorbent with zero point charge. Increased adsorption capacity can result from a charged ZnO-rGO NC for removal of RhB at low pH value with the use of different adsorbents**.**

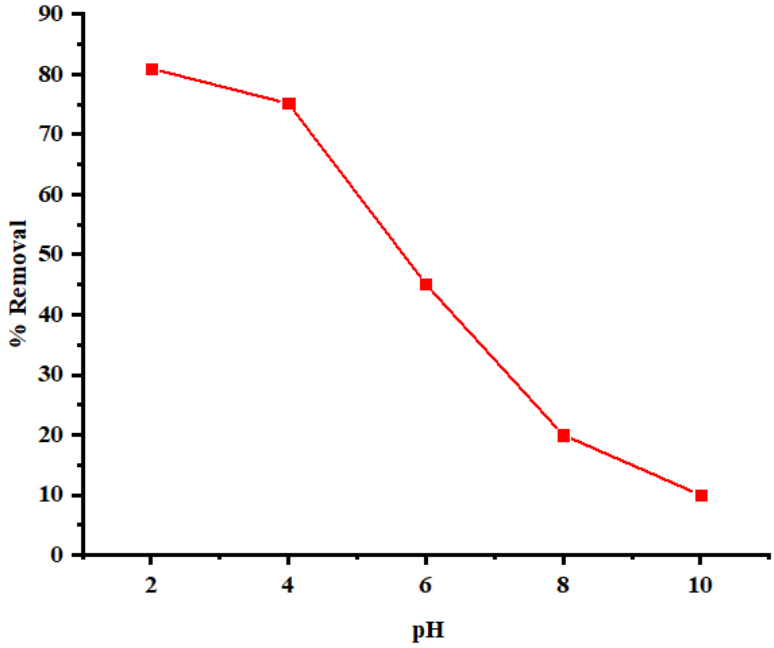

Figure 12. Effect of pH on the removal of RhB dye

4. ISOTHERMS ADSORPTION

4.1 Langmuir Adsorption Isotherm

Knowing the isotherm of the state of equilibrium of the adsorbents is essential for explaining the adsorption process [38-40]. It is crucial to determine the absorptivity of the adsorbents at various starting adsorbate concentrations. Analyzing the data from different solution concentrations has allowed models of the adsorption isotherms to be established. Considering related adsorbing sites are present for this work, the Langmuir adsorption models recommended monolayer-layered adsorption within limiting absorption. To compute the maximal adsorption capacity for the whole monolayer covering of the adsorbent surface, the Langmuir model was employed [41].

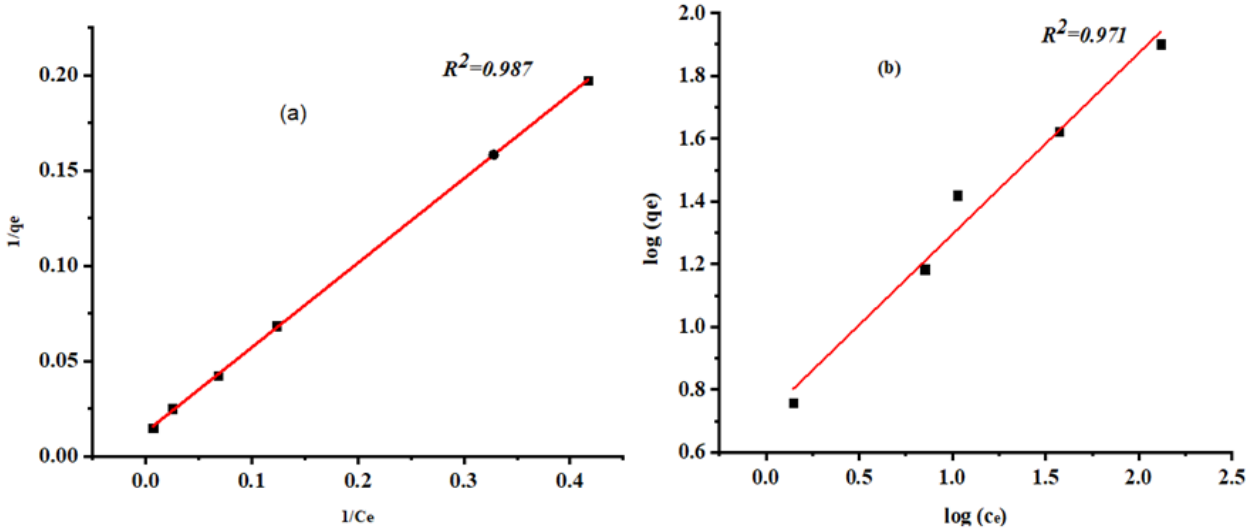

*Figure 13. Plot of (a) Langmuir isotherm and (**b**) Freundlich isotherm Model*

For the Langmuir isotherm model, homogenous adsorbent surfaces and proportional sorption energies for every sorbent spot have been hypothesized. Generally, gas-solid phase adsorption is described by the Langmuir isotherm model, which makes an inference that monolayer adsorption, occurs at a particular, localized site. Both uniform (*enthalpies and sorption activation energies of molecules*) are supported by this model for homogenous adsorption. The expression for the Langmuir isotherm model is given by Eq. (5) [42], and it consists of an equilibrium saturation point and a point of elevation.

$$q_e = \frac{qmaxKLce}{\frac{1}{kLce}} \qquad (5)$$

Here, k_L stands for the Langmuir constant and *Ce* is the dye concentration at the equilibrium stage. The produced adsorbents' monolayer capacity is denoted by q_{max}. The linear plot of *Ce* and *Ce/qe* in Fig. 13a can be used to determine the constants k_L and q_{max} based on their slope and intercept.

4.2 Freundlich Adsorption isotherm

By using the Freundlich isotherm model on the provided data, it is possible to find any potential heterogeneous assemblages on the adsorbent surfaces [43, 44]. The Freundlich isotherm model is a widely used explanation of adsorptions considered reversible and non-ideal. This model supports the various adsorption layers over the diverse surface of the adsorbent. The value close to zero or the area of the slope between 0 and 1 indicates the degree of adsorption or surface heterogeneity; a larger value indicates a broader surface. The chemical adsorption procedure is assumed if the adsorption rate (1/n) value is lower than 1, and a cooperative approach is demonstrated if it is larger than 1. The Freundlich isotherm model is described by equation (6), which is as follows:

$$q_e = k_F c_e 1/n \qquad (6)$$

K_F informs the adsorption capacity in this case. One possible value for the isotherm type is 1/n. A number ranging from 0 to 1/n < 1 indicates a

favorable isotherm. A number of 0 implies an irreversible isotherm, whereas a value larger than 1 denotes an unfavorable isotherm in Figure 13b.

Table 2. Parameters of various models on adsorption of RhB Dye using ZnO-rGO NC adsorbents

Nanocomposite	Type of model	Parameters	
ZnO-rGO	Langmuir	k_L(L/mg)	R^2
		0.029	0.999
	Freundlich	k_f	R^2
		5.220	0.971

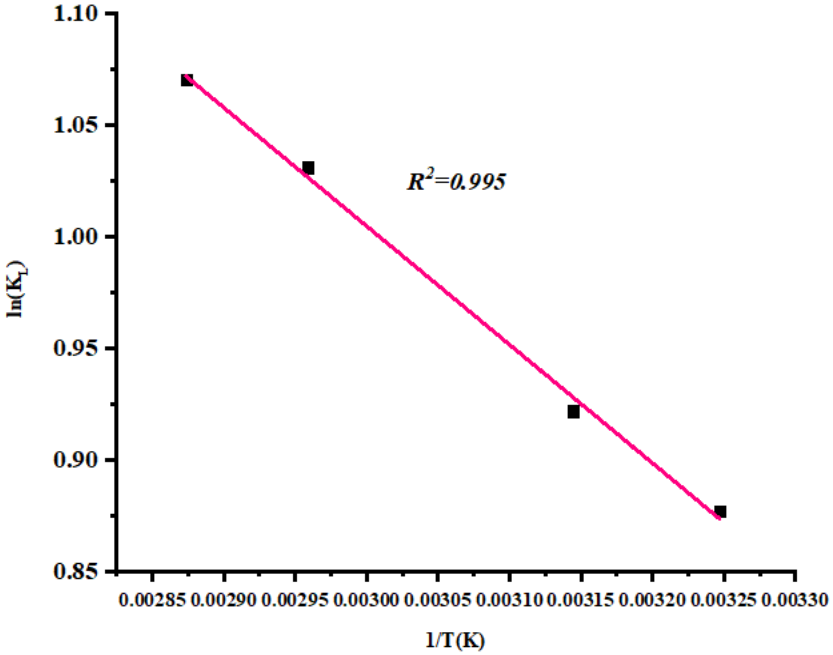

Figure 14. Plots of thermodynamics for RhB dye Adsorption

It was discovered that RhB dye adsorption onto ZnO-rGO NC had a ΔS° of (– 21.59 kJ/mol). Throughout the whole adsorption process, the solid solution interface's uncertainty level of freedom decreases, as indicated by the negative number. Additionally, it was noted that while adsorptive capabilities marginally declined, the ejection of the dye increased as reaction temperature increased (308—348 K) (Fig. 14).

Table 3. Thermodynamic Parameters for RhB Dye Adsorption onto ZnO-rGO NC

T(K)	Ce (L/mg)	KL	ΔG (kJ/mol)	ΔS (J/mol)	ΔH kJ/(mol K)
308	2.4	2.404	-2.246	-21.59	4.41
318	8.1	2.514	-2.437		
338	14.6	2.804	-2.897		
348	40.2	2.216	-3.096		

5. THERMODYNAMICS STUDIES

In addition to estimating the thermodynamic parameters, this study looked into the impact of reaction temperature on RhB dye removal utilizing synthesized ZnO-rGO NC. The spontaneous and thermodynamically feasible RhB dye adsorption onto the synthesized ZnO-rGO NC is indicated by the negative values of ΔG° [45]. The exothermic nature of sorption is demonstrated by the negative enthalpy (ΔH°) of the RhB dye adsorption (−4.41) displayed in Table 3**.**

6. CONCLUSION

This research dealt with the novel synthesis of ZnO nanoparticles from C. papaya leaf while rGO nanoparticles were produced using a modified Hummer's method. Following the synthesis of ZnO and rGO, FESEM and XRD for ZnO-rGO NC were recorded while FTIR for ZnO NPs was carried out. A straightforward ultrasonic technique was used to load ZnO onto rGO, creating a ZnO-rGO nanocomposite. The removal of RhB dye peaked at pH 2 and decreased at pH 10. The rGO-ZnO nanocomposite was also discovered to have a lot of potential for use as an efficient RhB removal from an aqueous medium. Because most contaminants are redistributed from aqueous media using chemicals, green synthesis offers a treatment because it is economical, low-cost, and

environmentally beneficial. Further, there is a need to carry out a real world application using polluted water in future application to investigate the effectiveness of the adsorbent, hence, its significance.

Acknowledgment

Sincere gratitude and admiration are extended to Km. Rachna for her supervisory role and S. Shankara Narayanan for the laboratory guidance and the enormous partnership. Your contributions and tireless efforts are duly acknowledged; thank you.

7. REFERENCES

[1] D. López-Rodríguez, Micó-Vicent, J. Jordan Nunez, M. Bonet-Aracil, E. Bou-Belda (2021) Uses of Nanoclays and Adsorbents for Dye Recovery: A Textile Industry Review. *Appl. Sci.* (11), (11422. doi: 10.3390/app112311422

[2] Y.Tu, G. Shao, W. Zhang, J. Chen, Y. Qu, F. Zhang, S. Tian, Z. Zhou, Z. Ren (2022) The degradation of printing and dyeing wastewater by manganese-based catalysts. *Sci. Total Environ.* (828), 154390. doi: 10.1016/j.scitotenv.2022.154390

[3] N.Hajipour, M.Ghorbanpour, M.Safajou-Jahankhanemlou (2022) Synthesis and characterization of solid-state Fe-exchanged nano-bentonite and evaluation of methyl orange adsorption. *Environ. Sci. Pollut. Res.* (29), 49898–49907. doi: 10.1007/s11356-022-19326-4

[4] A.K.D. Alsukaibi (2022) Various Approaches for the Detoxification of Toxic Dyes in Wastewater. *Processes.* (10), 1968. doi: org/10.3390/pr10101968

[5] N. Serpone, A.V. Emeline (2012) Semiconductor photocatalysis— past, present, and future outlook. *J. Phys. Chem. Lett*. (3), 673–677. doi: org/10.1021/JZ300071J/ASSET/

[6] Di.Mauro, A.Fragala, M.E.Privitera, V.G. Impellizzeri (2017) ZnO for application in photocatalysis: from thin films to nanostructures. *Mater. Sci. Semicond. Process*. (69), 44–51. doi: org/10.1016/J.MSSP.2017.03.029

[7] U.Özgür, I.Ya.Alivov, C.Liu, A.Teke, M.A. Reshchikov, S.Doğan, V.Avrutin, S.J.Cho, H. Morkoç (2005) A comprehensive review of ZnO materials and devices, *Journal of Applied Physics* 98, 041301. doi: org/10.1063/1.1992666

[8] J. Tian, Q. Zhang, L. Zhang, R. Gao, L. Shen, Sh. Zhang, X. Qu, G. Cao (2013) ZnO/TiO_2 nanocable structured photo electrodes for CdS/CdSe quantum dot co-sensitized solar cells, Nanoscale (5) 936–943. doi: 10.4028/www.scientific.net/amr.873.556

[9] S.Talam, R.K.Srivinasa, G.Nagarjuna (2012) Synthesis, characterization, and spectroscopic properties of ZnO nanoparticles. *IRSN Nanotechnol,* 1–6. doi: 10.5402/2012/372505

[10] N.T.Nguyen, V.A.Nguyen (2020) Synthesis, Characterization, and Photocatalytic Activity of ZnO Nanomaterials Prepared by a Green, Nonchemical Route. *J. Nanomater.* 1–8. doi:10.1155/2020/1768371

[11] J.C.G. Sousa, A.R. Ribeiro, M.O. Barbosa, M.F.R. Pereira, A.M.T.Silva (2018) A Review on Environmental Monitoring of Water Organic Pollutants Identified by EU Guidelines. *J. Hazard. Mater.* (344), 146–162. doi: 10.1016/j.jhazmat.2017.09.058

[12] A.E. Moharm, G.A. Naeem, H.M.A.Soliman, A.I. Abdelhamid, A.A. Elbardan, T.S. Kassem, A.A. Nayl, S. Brase (2022) Fabrication and Characterization of Effective Biochar Biosorbent Derived from Agricultural Waste to Remove Cationic Dyes from Wastewater. *Polymers.* (14), 2587. doi: org/10.3390/polym14132587

[13] S.H. Ferreira, M.Morais, D. Nunes, M.J.Oliveira, A. Rovisco, A. Pimentel (2021) High UV and Sunlight Photocatalytic Performance of Porous ZnO Nanostructures Synthesized by a Facile and Fast Microwave Hydrothermal Method. *Materials* (14), 2385. doi: 10.3390/ma14092385

[14] D. Luo, L. Wang, H. Nan, Y. Cao, H. Wang, T.V. Kumar, C. Wang (2022) Phosphorus adsorption by functionalized biochar: A review. Environ. *Chem. Lett.* (21), 497–524. doi.10.1007/s10311-022-01519-5

[15] F. Zhao, R. Shan, J. Gu, Y. Zhang, H. Yuan, Y. Chen (2022) Magnetically Recyclable Loofah Biochar by $KMnO_4$ Modification for Adsorption of Cu(II) from Aqueous Solutions. *ACS Omega.* (7), 8844–8853. doi.org/10.1021/acsomega.1c07163

[16] K.S.D. Premarathna, A.U. Rajapaksha, N. Adassoriya, B. Sarkar, N.M. Sirimuthu, A. Cooray, Y.S. Ok, M. Vithanage (2019) Clay-biochar composites for sorptive removal of tetracycline antibiotic in aqueous media. *J. Environ. Manag.* (238), 315 322. doi: 10.1016/j.jenvman. 2019. 02.069

[17] P.Jaiswal, P.Kumar, V.K. Singh, D.K. Singh (2010) Carica papaya Linn: A potential source for various health problems. *Journal of Pharmacy Research*, *3*(5), pp.998-1003.

[18] M.H. Koupaei, B. Shareghi, A.A. Saboury, F. Davar, A. Semnani, M. Evini (2016) Green synthesis of zinc oxide nanoparticles and their effect on the stability and activity of proteinase K. *RSC advances*, *6*(48), pp.42313-42323. doi: org/10.1039/C5RA24862K

[19] B. Kumar, K. Smita, L. Cumbal, A. Debut (2014) Green approach for fabrication and applications of zinc oxide nanoparticles. *Bioinorganic chemistry and applications*. doi: org/10.1155/2014/523869

[20] J. Qu, X. Yuan, X. Wang, P. Shao (2011) Zinc accumulation and synthesis of ZnO nanoparticles using Physalis alkekengi L. *Environmental pollution*, *159*(7), pp.1783-1788. doi: org/10.1016/j.envpol.2011.04.016

[21] J. Qu, C. Luo, J. Hou (2011) Synthesis of ZnO nanoparticles from Zn-hyper accumulator (Sedum alfredii Hance) plants. *Micro & Nano Letters*, *6*(3), pp.174-176. doi: 10.1049/mnl.2011.0004

[22] H.J. Lee, G. Lee, N.R. Jang, J.H. Yun, J.Y. Song, B.S. Kim (2011) Biological synthesis of copper nanoparticles using plant extract. *Nanotechnology*, *1*(1), pp.371-374. doi: 10.3390/polym13244364

[23] H.U. Lee, K. Ahn, S.J. Lee, J.P. Kim, H.G. Kim, S.Y. Jeong, C.R. Cho (2011) ZnO Nano barbed fibers: fabrication, sensing NO_2 gas, and their sensing mechanism. *Applied Physics Letters*, *98*(19). doi:10.1063/1.3590202

[24] H.A. Salam, R. Sivaraj, R. Venckatesh (2014) Green synthesis and characterization of zinc oxide nanoparticles from Ocimum basilicum L. var. purpurascens Benth.-Lamiaceae leaf extract. *Materials letters*, *131*, pp.16-18. doi: org/10.1016/j.matlet.2014.05.033

[25] AH. Agarwal, S.V. Kumar, S. Rajeshkumar (2017) A review on green synthesis of zinc oxide nanoparticles–An eco-friendly approach. *Resource-Efficient Technologies*, *3*(4), pp.406-413.doi: 10.1016/j.reffit.2017.03.002

[26] A.J. Love, V.V. Makarov, O.V.Sinitsyna, J.Shaw, I.V. Yaminsky, N.O. Kalinina, M.E. Taliansky, (2015) A genetically modified tobacco mosaic virus that can produce gold nanoparticles from a metal salt precursor. *Frontiers in plant science*, *6*, p.984. doi: org/10.3389/fpls.2015.00984

[27] A.Happy, M.Soumya, S.Venkat Kumar, S. Rajeshkumar, N.D.Sheba Rani, T.Lakshmi, V. Deepak Nallaswamy (2019) Phyto-assisted synthesis of zinc oxide nanoparticles using Cassia alata and its antibacterial activity against Escherichia coli. Biochem. *Biophys. Rep.* doi: org/10.1016/j.bbrep.2019. 01.002.

[28] J. Suresh, G. Pradheesh, V. Alexramani, M. Sundrarajan, S.I. Hong (2018) Green synthesis and characterization of zinc oxide nanoparticle using insulin plant (Costus pictus D. Don) and investigation of its antimicrobial as well as anticancer activities. *Adv. Nat. Sci.* doi: org/10.1088/2043-6254/ aaa6f1.

[29] B.J. Li, H.Q. Cao (2011) ZnO @graphene composite with enhanced performance for the removal of dye from water, *J. Mater. Chem.* (21) 3346–3349. doi.org/10.1039/C0JM03253K

[30] J. Jayachandiran, J. Yesuraj, M. Arivanandhan, A. Raja, S.A. Suthanthiraraj, R. Jayavel, D.J.J.O.I. Nedumaran (2018) Synthesis and electrochemical studies of rGO/ZnO nanocomposite for supercapacitor application. *Journal of Inorganic and Organometallic Polymers and Materials*, (28), 2046-2055. doi: 10.1007/s10904-018-0873-0

[31] Khatoon, N. Khan, A.H. Pathak, V. Agnihotri, N. Rehman (2013) Removal of Hexavalent Chromium from syntheticwaste water using synthetic nano zero valentIron (NZVI) as adsorbent. *Int. J. Innov. Res. Sci. Eng. Technol*. 2 (11), 6140–6149.

[32] K.Dulta, G.Koşarsoy Ağçeli, P.Chauhan, R. Jasrotia, P.K. Chauhan (2021) Ecofriendly synthesis of zinc oxide nanoparticles by Carica papaya leaf extract and their applications. *Journal of Cluster Science*, 1-15.doi:org/10.1007/s10876-020-01962-w

[33] L. Kaliraj, J.C. Ahn, R.J. Rupa, S. Abid, J. Lu, and D.C. Yang (2019) Synthesis of panos extract mediated ZnO nano-flowers as photocatalyst for industrial dye degradation by UV illumination. *Journal of Photochemistry and Photobiology B: Biology*, (199),111588.
doi: org/10.1016/j.jphotobiol.2019.111588

[34] K. Davis, R. Yarbrough, M. Froeschle, J. White, H. Rathnayake (2019) Band Gap Engineered Zinc Oxide Nanostructures: Via a Sol-Gel Synthesis of Solvent Driven Shape-Controlled Crystal Growth. *RSC Adv.* 9 (26), 14638–14648. doi.org/10.1039/C9RA02091H

[35] H. Aysan, S. Edebali, C. Ozdemir, M.C. Karakaya, N. Karakaya (2016) Use of chabazite, a naturally abundant zeolite, for the investigation of the adsorption kinetics and mechanism of methylene blue dye. *Microporous Mesoporous Mater*. (235), 78–86. doi: org/10.1016/j.micromeso.2016.08.007

[36] X. Zhang, C. Cheng, J. Zhao, L. Ma, S. Sun, C. Zhao (2013) Polyethersulfone enwrapped graphene oxide porous particles for water treatment. *Chem. Eng. J*. 215–216, 72–81. doi: org/10.1016/ j.cej.2012.11.009

[37] R. Kamaraj, S. Vasudevan (2015) Evaluation of electrocoagulation process for the removal of strontium and cesium from aqueoussolution. *Chem. Eng. Res. Des*. (93), 522–530. https://doi.org/ 10.101 6/j.cherd.2014.03.021

[38] R. Kamaraj, P. Ganesan, S. Vasudevan (2015) Removal of lead from aqueous solutions by electrocoagulation: isotherm, kinetics and thermo-dynamic studies. *Int. J. Environ. Sci. Technol.* 12, 683–692. doi: org/10.1007/s13762-013-0457-z

[39] S. Vasudevan, J. Lakshmi, G. Sozhan (2012) Optimization of electrocoagulation process for the simultaneous removal of mercury, lead, and nickel from contaminated water. *Environ. Sci. Pollut. Res*. (19), 2734–2744. doi: org/10.1007/s11356-012-0773-8

[40] S.Vasudevan, J.Lakshmi, G.Sozhan (2012) Simultaneous removal of Co, Cu, and Cr from water by electrocoagulation. *Toxicol. Environ. Chem*. 94(10), 1930–1940. doi: org/10.1080/027722 48.2012.742898

[41] J.C. Igwe, A.A. Abia (2006) Abioseparation process for removing heavy metals from waste water using biosorbents. *Afr. J.* Biotechnol. (5), 1167–1179.

[42] I. Langmuir (1918) the adsorption of gases on plane surfaces of glass, mica and platinum. *J. Am. Chem. Soc*. (40), 1361–1403. doi: org/10.1021/ ja02242a004

[43] S. Vasudevan, J. Lakshmi, M. Packiyam (2010) Electrocoagulation studies on removal of cadmium using magnesium electrode. *J. Appl. Electrochem.* (40), 2023–2032. https://doi.org/10.10 07/s10800-010-0182-y

[44] S.Vasudevan, G.Sozhan, S. Ravichandran, J. Jayaraj, J. Lakshmi, S.M. Sheela, (2018) Studies on the removal of phosphate from drinking water by electrocoagulation process. *Ind. Eng. Chem. Res*. (47), 2018–2023. doi: org/10.1021/ie0714652

[45] S.Vasudevan, J. Lakshmi, G. Sozhan (2011) Effects of alternating and direct current in electrocoagulation process on the removal of cadmium from water. *J. Hazard. Mater.* (192), 26–34. doi: org/10.1016/j.jhazmat.2011.04.081

IZVOD

LAKA SINTEZA I ADSORPTIVNO UKLANJANJE RODAMINA B BOJE IZ VODENE SREDINE KORIŠĆENJEM ZELENOG SINTETIZOVANOG NANOKOMPOZITA

Redukovani grafen oksid (rGO) i nanočestice cinkoksida (ZnO NP) su sintetizovane korišćenjem modifikovane Hamerove metode i zelene sinteze iz ekstrakta lista Carica papaje (CPLE), respektivno. ZnO NP su zatim napunjeni na rGO korišćenjem jednostavne ultrazvučne metode za sintetizu nanokompozita grafen oksida redukovanog cink oksidom (ZnO-rGO NC). Infracrvena spektroskopija sa Furijeovom transformacijom (FTIR), emisiona skenirajuća elektronska mikroskopija (FESEM) i difrakcija rendgenskih zraka (XRD) su korišćene za karakterizaciju sintetizovanih nanočestica i kompozita. Nanokompozit je korišćen za uklanjanje Rhodamine B boje (RhB) iz vodenog rastvora. Ispitivani su uticaji temperature, pH, doze adsorbenta, početne koncentracije boje i vremena kontakta. Ispitivanje je takođe obavljeno na modelima Freundlich i Langmuir izoterme i izračunati su termodinamički parametri. Urađeni su i prikazani efekti ZnO NP, rGO i ZnO-rGO NC nezavisno na uklanjanje boje u komparativnoj analizi. U vodenom medijumu, nanokompozit je pokazao visoku efikasnost kao adsorbent za uklanjanje RhB boje sa 99% u poređenju sa ZnO NP sa 60%.

Ključne reči: *Adsorpcija, ZnO nanočestice, nanokompoziti, zagađivači, rodamin B, redukovani grafen oksid, carica papaja*

Naučni rad
Rad primljen: 13.01.2024.
Rad prihvaćen: 19.02.2024.
Rad je dostupan na sajtu: www.idk.org.rs/casopis

Flomo L. Gbawoquiya https://orcid.org/0009-0009-7775-6651
Kumari Rachna[1] https://orcid.org/0000-0003-0670-5362
Shankara S. Narayanan https://orcid.org/0000-0002-5092-3263
Pramod K. Singh https:/orcid.org/0000-0002-3155-6621
Shiv Shankar https://orcid.org/0000-0001-8082-8243
Ikhwan Syafiq Mohd Noor https://orcid.org/0000-0003-0983-782x
Muhd Zu Azhan Yahya https://orcid.org/0000-0003-1129-0552